Macromolecules

Article

pubs.acs.org/Macromolecules

Nanoparticle Brush Architecture Controls Polymer Diffusion in Nanocomposites

Jihoon Choi,[†] Michael J. A. Hore,[‡] Nigel Clarke,[§] Karen I. Winey,[†] and Russell J. Composto*[,†]

[†]Department of Materials Science and Engineering, University of Pennsylvania, Philadelphia, Pennsylvania 19104, United States

[‡]Center for Neutron Research, National Institute of Standards and Technology (NIST), 100 Bureau Drive, Gaithersburg, Maryland 20899, United States

[§]Department of Physics and Astronomy, University of Sheffield, S3 7RH, United Kingdom

Supporting Information

ABSTRACT: We show that polymer diffusion in polymer nanocomposites (PNCs) is controlled by the architecture of polymer brushes grafted to hard spherical nanoparticles (NPs). At high grafting density, diffusing chains are excluded from the polymer brush leading to greater confinement. However, at lower grafting density, these chains penetrate the brush and diffusion is similar to the hard NP case, compared at the same NP loading. We calculate the effective interparticle spacing (ID_{eff}) by modeling polymer penetration into the grafted brush using self-consistent field theory. When plotted against a confinement parameter ($ID_{eff}/2R_g$, where R_g is the radius of gyration of the diffusing polymer), reduced diffusion coefficients (D/D_o) fall on a master curve independent of brush architecture. These findings show that brush architecture provides a new route toward controlling polymer dynamics and viscoelasticity of PNCs.

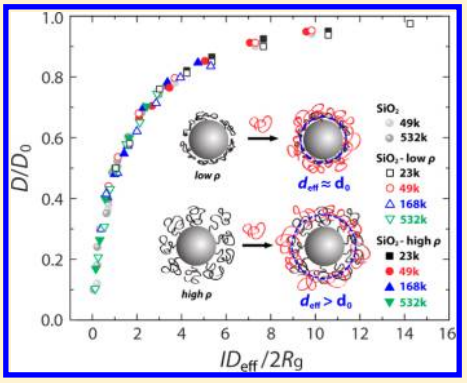

INTRODUCTION

The effect of nanoconfinement on polymer dynamics is fundamentally important for understanding diffusion and glasses, and practically important for applications ranging from microelectronics to biosensors.[1,2] In addition to polymers confined in nanopores and thin films, polymers mixed with nanoparticles (NPs), namely polymer nanocomposites (PNC), can experience confinement even at low loadings, ~1 vol %.[3−5] A unifying theoretical picture that captures the effect of nanoparticles on polymer dynamics has yet to emerge, in part, because of the numerous system parameters including polymer type, polymer molecular weight, NP size, NP shape, NP concentration, polymer-NP interactions, polymer entanglement, and NP packing. To control the dispersion of NPs, NP surfaces are typically grafted with either short molecules or long polymer brushes.[6−9] In the latter case, the grafted NPs can act as either hard or soft NPs depending on whether the matrix chains are excluded or can penetrate the brush, respectively. Penetration of matrix polymers into the polymer brush depends on brush architecture, namely, molecular weight and grafting density, which impact whether the NPs disperse or aggregate in a particular matrix polymer.[10] Whereas recent studies have focused on polymers mixed with hard NPs,[6,7,11,12] polymer diffusion in PNCs containing soft NPs has received little attention despite the common use of surface functionalization to enhance NP miscibility in PNCs.[5] Moreover, systematic studies of diffusion of high molecular weight polymers in PNCs containing soft NPs are lacking.

In this paper, we demonstrate that the center-of-mass diffusion of polymers in PNCs containing soft and hard NPs collapses onto a master curve when plotted against a confinement parameter. This parameter reduces the complexity of the diffusing species and matrix into a dimensionless confinement parameter by combining the diffusing chain's radius of gyration (R_g), NP size, and NP concentration into a single parameter. Previously, we have focused on polymer diffusion in PNCs containing hard NPs such as phenyl-capped and hydroxyl terminated silica.[13,14] More recently, we have investigated diffusion into PNC's containing soft, large (51 nm) NPs grafted at high density (0.52 chains/nm^2) with a long brush (M_n = 87 kg mol^{-1}).[5] These earlier studies show that low molecular weight tracer molecules penetrate the brush and have diffusion coefficients identical to the hard NP case at the same silica loading.[5] In this paper, we show that the confinement parameter ($ID_{eff}/2R_g$) unifies experimental observations of both long and short chain polymer diffusion in PNCs containing either hard or soft nanoparticles. Unique to the current study, we show that long, entangled tracer polymers (i.e., M_n = 532 kg mol^{-1}) are excluded from the polymer brush of soft NPs (29 nm) with high grafting density and that at fixed silica loading diffusion is slowed down by up to 60% compared to hard NPs. In contrast, for PNCs containing soft NPs with low grafting density, long (M_n = 532 kg mol^{-1}) and short (M_n = 49 kg

Received: January 30, 2014
Revised: March 10, 2014
Published: March 19, 2014

   dx.doi.org/10.1021/ma500235v | *Macromolecules* 2014, 47, 2404−2410

mol^{-1}) tracer polymers exhibit diffusion coefficients similar to the hard NP case because the tracer penetrates into the brush. The diversity of PNCs in which polymer diffusion correlated with the confinement parameter is compelling and is likely to inspire broadly applicable theories of polymer dynamics in nanocomposites.

THEORETICAL METHODS

Self-Consistent Field Theory (SCFT). SCFT has been successful in describing many polymer systems, such as those composed of block copolymers and nanoparticles. Here, we take the same approach as in a recent paper[15] and use a SCFT to determine the degree to which a tracer polymer penetrates into the brush of a polymer-grafted nanoparticle. The partition function for such a system, which contains n_b brush chains, n_m matrix chains, and n_t tracer chains is given by

$$Z = \int \prod_{i=1}^{n_b} DR_{i,b}(s) \int \prod_{j=1}^{n_m} DR_{j,m}(s) \int \prod_{k=1}^{n_t} DR_{k,t}(s) \exp(-\beta U_0[R_{i,b}(s)] - \beta U_0[R_{j,m}(s)] - \beta U_0[R_{k,t}(s)]) \delta[1 - \hat{\varphi}_b - \hat{\varphi}_m - \hat{\varphi}_t] \quad (1)$$

where U_0 is a harmonic potential between monomers and the delta functional enforces the incompressibility of the system. Since this partition function is numerically and analytically intractable, it is transformed into a partition function that is described by a single "pressure-like" auxiliary field ω_+:

$$Z = \int D\omega_+ \exp(-H[\omega_+]) \quad (2)$$

where the effective Hamiltonian H is

$$\frac{H}{k_B TC} = -\frac{1}{V} \int \mathrm{d}r\, [i\omega_+(r)] - \varphi_b \ln Q_b - \varphi_m \alpha_m^{-1} \ln Q_m - \varphi_t \alpha_t^{-1} \ln Q_t \quad (3)$$

Additional details regarding our SCFT are available in two recent publications.[5,15] Unlike our previous calculations, however, the brush grafting points are smeared which assists in relaxation of the pressure field.[16]

A mean field approximation is imposed on the Hamiltonian, such that at equilibrium the Hamiltonian is described by a single field configuration ω_+^* To relax the field to its equilibrium value, a semi-implicit Seidel (SIS) scheme is used, which has resolution and stability advantages over a more standard explicit Euler update scheme.[17] The SIS scheme is the result of expanding the density operators to linear order in ω_+ using the random phase approximation (RPA), and adding and subtracting the linear terms of the expansion at the present and future time step, respectively, to obtain:

$$\frac{\omega_+^{n+1} - \omega_+^n}{\Delta t} = -g^* \omega_+^{n+1} - \frac{\partial H[\omega_+^n]}{\partial \omega_+^n} + g^* \omega_+^n \quad (4)$$

where the $*$ operator represents a convolution. We implement this scheme in Fourier space, as the convolution is a simple multiplication operation in Fourier space. In Fourier space, $g(k) = \varphi_b F_D(k^2) + \varphi_m F_D(\alpha_m k^2) + \varphi_t F_D(\alpha_t k^2)$, where F_D is the Debye scattering function. The SIS scheme is performed at each iteration of the calculation until the error in ω_+,

$$\text{error} = \frac{1}{M^2} \sum_{i=1}^{M^2} |1 - \varphi_b(r_i) - \varphi_m(r_i) - \varphi_t(r_i)| \quad (5)$$

is less than 10^{-6}.

EXPERIMENTAL METHODS

Particle Synthesis. Silica nanoparticles were obtained from Sigma-Aldrich (Ludox) and functionalized with the alkyl halide initiator 1-(chlorodimethylsilyl)propyl-2-bromoisobutyrate according to a procedure described previously, and denoted as SiO_2 (hard NP).[18,19] The particle diameter and polydispersity were measured by dynamic light scattering (d_0 = 28.8 nm, σ = 1.13).[7] Styrene (Aldrich, 99%) was purified by passing through a basic alumina column. Copper(I) bromide (Aldrich, 98+%) was purified by washing sequentially with acetic acid and diethyl ether, filtering and drying, and was stored under vacuum before use. Allyl 2-bromo-2-methylpropionate, *N,N,N′,N″,N″*-pentamethyldiethylenetriamine (PMDETA), copper(II) brominde, anisole, and hydrofluoric acid (48%) were used as received from Aldrich. Synthesis of the soft particle system was performed using normal ATRP technique described in ref 20. Molecular weight and molecular weight distribution of surface-grafted chains were determined by size exclusion chromatography (SEC) coupled with an IR absorption detector after etching the silica with HF. Surface-grafting density was determined using thermogravimetric analysis (TGA). The number-average molecular weight (M_n^b), the polydispersity index (PDI), and the grafting density (ρ) of polymer brushes are summarized in Table 1. Polystyrene- (PS-) grafted silica nanoparticles

Table 1. Soft Nanoparticle Characteristics

name	M_n^b (g/mol)	PDI	ρ (nm^{-2})
SiO_2-low ρ	48 260	1.31	0.154
SiO_2-high ρ	85 930	1.24	0.383

with low and high grafting densities were denoted as SiO_2-low ρ and SiO_2-high ρ, respectively. Figure 1 depicts electron micrographs of the respective particle monolayer, revealing the dependence of the brush structure (i.e., interparticle spacing) on the molecular weight and grafting density.

Preparation and Characterization of Polymer Nanocomposites. Polystyrene (M_n^m = 160 kg mol^{-1}, PDI = 1.05) with the surface-functionalized silica nanoparticles (alkyl halide initiator or polystyrene) is used as a matrix. The volume fractions of SiO_2 (ϕ_{silica}) in PS are 0, 0.005, 0.01, 0.02, 0.04, 0.06, 0.1, 0.2, 0.29 for SiO_2-low ρ and 0, 0.005, 0.01, 0.02, 0.04, 0.06, 0.085 for SiO_2-high ρ, and 0, 0.005, 0.01, 0.02, 0.04, 0.06, 0.085, 0.1, 0.2, 0.3, 0.5 for SiO_2. The SiO_2-low ρ, SiO_2-high ρ, and SiO_2 were mixed at the appropriate ratio with PS. Films were prepared by doctor blading the solution on a heated glass substrate (~120 °C) to form a film of thickness ~10 μm. The dispersion of nanoparticles was observed using TEM (JEOL 2010 operated at 200 kV) after cross-sectioning the films using a microtome.

Tracer Diffusion Couple and Processing. The tracer diffusion couples consisted of the nanocomposite matrix film covered with ~20 nm thick dPS tracer film. Four different molecular weights of dPS (23 kg mol^{-1}, PDI = 1.06; 49 kg mol^{-1}, PDI = 1.03; 168 kg mol^{-1}, PDI = 1.03; 532 kg mol^{-1}, PDI = 1.05) were used as a tracer. The radius of gyration (R_g) was calculated using a segment size of 0.67 nm. The dPS film was spin coated on silicon substrates and floated off in water and transferred onto the matrix film placed on the silicon substrate. The diffusion couples were annealed in a vacuum oven at 170 °C.

Elastic Recoil Detection (ERD). In ERD the He^{2+} ion beam was accelerated to 3 MeV and intersects the plane of the sample at 15°. A 10 μm Mylar film was placed in front of the ERD detector to prevent the signal from the forward scattered He from masking the H and D signal, and the recoiled H and D are collected by a solid-state detector. The dPS volume fraction profile converted from the ERD spectra of counts versus channel using the thin slab approach was fitted by a convolution of the appropriate solution to Fick's second law with a

dx.doi.org/10.1021/ma500235v | Macromolecules 2014, 47, 2404−2410

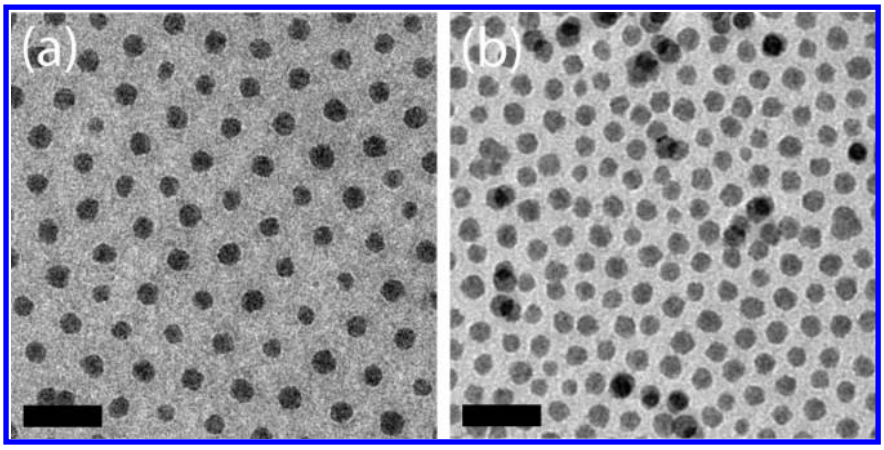

Figure 1. Transmission electron micrographs depicting monolayer of polystyrene-grafted silica nanoparticles with (a) high and (b) low grafting densities, respectively. Scale bar is 100 nm.

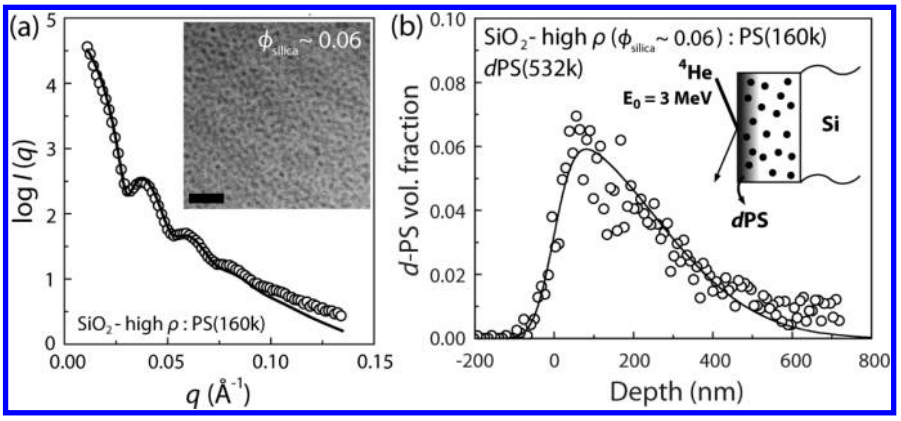

Figure 2. (a) Morphology of SiO_2-high ρ:PS nanocomposite (ϕ_{silica} = 0.06) and corresponding SAXS scattering curve. Cross-sectional TEM micrograph (inset) depicts the distribution of SiO_2 cores in the PS matrix (M_n^m = 160 kg mol^{-1}). Scale bar is 200 nm. The solid line is the best fit using the Rayleigh function (d_0 = 28 nm). (b) Representative volume fraction profile of dPS(532k) in SiO_2-high ρ:PS (ϕ_{silica} = 0.06). Solid line is a fit of the depth profile using Fick's second law with $D = 1.03 \times 10^{-14}$ cm^2 s^{-1}.

Gaussian function that represents the instrumental resolution. For more detailed information the reader is referred to the specialized review.[21]

RESULTS AND DISCUSSION

A uniform dispersion of NPs is essential so that the average ID for a random distribution of NPs can be calculated from the NP diameter and volume fraction.[14] The SAXS measurement and cross-sectional transmission electron micrograph in Figure 2a show that NPs are well dispersed in the PS matrix at ϕ_{silica} = 0.06.[22] The surface modifications of these hard and soft NPs facilitate their uniform dispersion in PS even up to extremely high loading for SiO_2 NPs, ϕ_{silica} = 0.5 (Figure S1a-c). Furthermore, SAXS spectra confirm that NPs with different surface modification exhibit nearly identical dispersion in the PS matrix (Figure S 1d).

Figure 2b shows a representative dPS volume fraction profile where the solid line is the best fit to the experimental data (circles). Using Fick's second law and appropriate boundary and initial conditions, $\phi_{dPS}(x)$ is given by

$$\phi_{dPS}(x) = \frac{1}{2}\left[\mathrm{erf}\left(\frac{l-x}{\sqrt{4Dt}}\right) + \mathrm{erf}\left(\frac{l+x}{\sqrt{4Dt}}\right)\right] \quad (6)$$

where erf, t, l, and D are the error function, annealing time, initial dPS thickness, and diffusion coefficient of dPS, respectively.[18] To determine D, $\phi_{dPS}(x)$ from Ficks second law is convoluted with the instrumental depth resolution and chi squared fitting is used to achieve the best fit between experimental (circles) and calculated (solid line) profiles.[23,24]

Figure 3 shows the tracer diffusion coefficients for dPS as a function of the volume fraction of silica. The trends between diffusion coefficient and parameters that define confinement, including dPS molecular weight and ID (i.e., silica volume fraction), are consistent with the previous diffusion studies in matrices with the immobile hard and grafted NPs:[5,7,13,14] (i) At fixed ϕ_{silica}, the diffusion coefficient decreases as the tracer molecular weight increases and (ii) as ϕ_{silica} increases, the diffusion coefficient also decreases for all tracer molecular weights, and (iii) a more pronounced decrease of the diffusion coefficient is observed for high molecular weight dPS (168k and 532k) compared to low molecular weight dPS (23k and 49k).

Compared to the hard NP system, polymer-grafted NPs present a tunable interfacial width that controls the ability of the matrix or tracer chains to penetrate the brush molecules.[25] Wijmans and Zhulina extended a mean-field lattice model, which describes polymer adsorption on planar surfaces, to determine the structure of polymer brushes under various solvent conditions.[26] This model was found to accurately capture the scaling behavior of polymer brushes of various architectures.[27] At high grafting density, excluded volume

dx.doi.org/10.1021/ma500235v | Macromolecules 2014, 47, 2404−2410

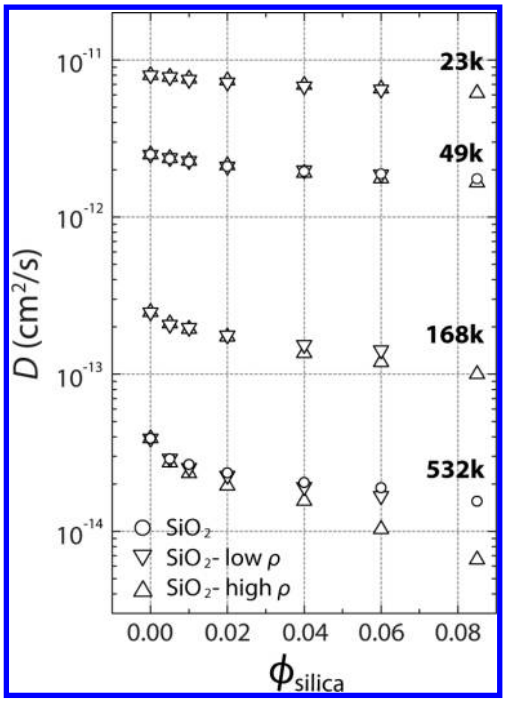

Figure 3. Tracer diffusion coefficients of dPS for M_n^t = 23, 49, 168, and 532 kg mol^{-1} in nanocomposites containing SiO_2, SiO_2-low ρ, or SiO_2-high ρ NPs at 170 °C as a function of the volume fraction of silica; open circles represent nanocomposites with SiO_2 NPs whereas the inverse triangles and triangles represent nanocomposites with SiO_2-low ρ and SiO_2-high ρ NPs, respectively.

interactions lead to extended chain conformations and expel matrix chains from the brush chains, particularly in the case of a high molecular weight matrix. At low grafting density when the brush and matrix chains are chemically identical, low molecular weight matrix chains readily penetrate into the brush. In short, the brush segment density as a function of radial distance from the particle surface depends on the grafting density, the brush molecular weight and the matrix molecular weight, as well as the nanoparticle size. Note that here SiO_2, SiO_2-low ρ, and SiO_2-high ρ NPs were prepared from the same silica nanoparticles.

The brush architecture defines the penetration depth of the tracer polymer and we see from Figure 3 that less penetration corresponds to slower diffusion, an effect that is magnified as the matrix molecular weight increases. For example, at low molecular weight dPS (23k and 49k), the tracer diffusion coefficients are nearly identical in PNCs with SiO_2, SiO_2-low ρ, or SiO_2-high ρ NPs because the extent of tracer penetration is comparable. In contrast at high molecular weight dPS (168k and 532k), tracer diffusion is slowest in the PNCs with SiO_2-high ρ NPs and fastest in the PNCs with SiO_2 NPs. This comparison suggests that larger tracer molecules have less accessible volume when diffusing in systems with SiO_2-high ρ NPs, because the dense polymer brush prohibits high molecular dPS from penetrating, and highlights the importance of brush architecture.

To elucidate the underlying relationship between polymer dynamics and brush structure, we compare dPS diffusion in PS matrices containing NPs with low (circle symbols) and high (square symbols) grafting densities *at equal silica loadings*. This effect is well demonstrated in Figure 4 where the tracer diffusion coefficient in the presence of these grafted NPs

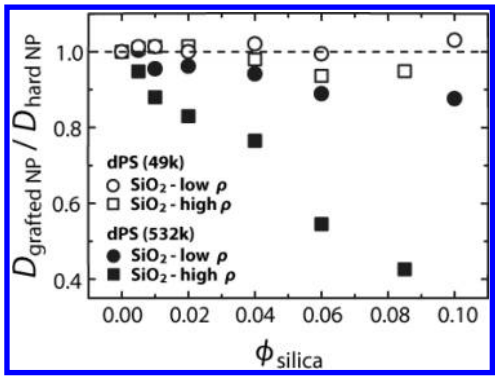

Figure 4. Effect of polymer brush grafting density on polymer diffusion in nanocomposites. Tracer diffusion coefficients ($D_{grafted\ NP}$) in PS-functionalized SiO_2:PS (SiO_2-low ρ:PS or SiO_2-high ρ:PS) normalized by tracer diffusion coefficients ($D_{hard\ NP}$) in short-ligand functionalized SiO_2:PS (SiO_2:PS) as a function of the volume fraction of silica. The relative diffusion coefficients of dPS are plotted for M_n^t = 49 (open symbols) and 532 (closed symbols) kg mol^{-1}.

($D_{grafted\ NP}$) is normalized by that in systems with SiO_2 NPs ($D_{hard\ NP}$). The diffusion of dPS(532k) in a PS matrix containing SiO_2-high ρ (closed squares) is much slower than in the NP with low ρ (closed circles); however, the diffusion coefficients for dPS(49k) are statistically similar in PNCs with SiO_2-low ρ and SiO_2-high ρ NPs (open circles and squares). These results indicate that any model describing polymer dynamics in nanocomposites, including the empirical confinement parameter, must account for the limited tracer penetration into the grafted brushes.

To quantify the dependence of the dPS penetration on the brush structure and grafting density, self-consistent field theory (SCFT) was used to determine the monomer density profiles of the brush, matrix, and tracer chains adjacent to the NP surface. These SCFT calculations of monomer density profiles were previously confirmed using small-angle neutron scattering (SANS) experiments, where the scattering length density profiles for the best SANS fit were in excellent agreement with the SCFT monomer density profiles.[5] Figure 5a and 5b show the profiles as a function of distance, normalized by the unperturbed brush size, for brushes of either SiO_2-low ρ or SiO_2-high ρ in contact with a mixture of the matrix PS(160k) and tracer dPS(168k) at φ_t = 0.1; see Supporting Information, Figure S2, for full SCFT results. The broad interface between brush (dashed−dotted) and matrix (dashed) chains results from the wetting of the PS matrix into the PS brush and is responsible for the excellent dispersion of SiO_2-high ρ in PS(160k) shown in Figure 2a. More wetting or penetration, in particular 50% of matrix monomers penetrating to the particle surface, is observed for the PS(48k) brush with low ρ (Figure 5a), because of a lower conformational entropy penalty for matrix chains to penetrate the sparsely grafted brushes, compared to the densely grafted brushes, PS(86k) with high ρ (Figure 5b). This wetting behavior is also observed for the tracer chains within the brush. For low grafting density (Figure 5a), dPS(168k) penetrates the brush fully, yielding an effective brush thickness, $h_{eff} \approx 0$. Thus, the tracer diffusion in PS matrices containing SiO_2-low ρ NPs should be similar to that for SiO_2 NPs, as shown in Figure 4 (SiO_2-low ρ, open circles). However, the identical dPS(168k) is excluded from the inner brush at high grafting density (Figure 5b), due to the entropic penalty associated with the overlap of crowded brush chains. As

dx.doi.org/10.1021/ma500235v | Macromolecules 2014, 47, 2404−2410

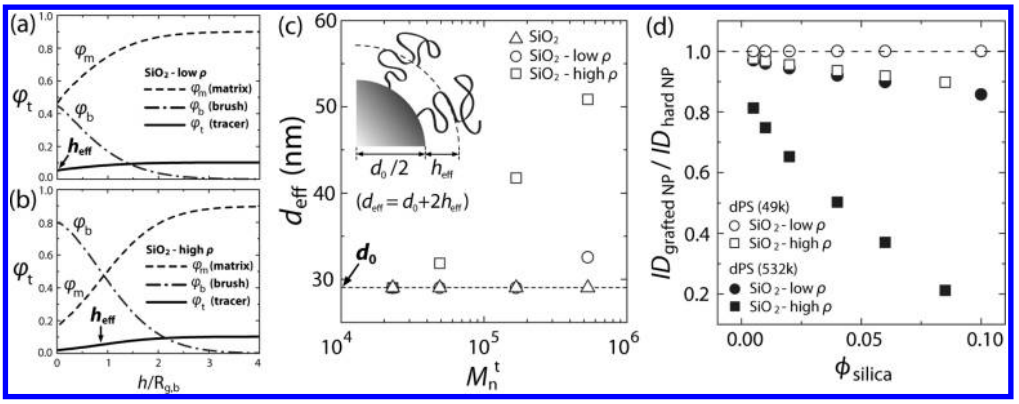

Figure 5. (a, b) Effect of surface grafting density on penetration of dPS(168k) tracer molecules into the PS brush grafted to NPs. Self-consistent field theory calculations showing the volume fraction profiles of dPS(168k) for (a) SiO_2-low ρ and (b) SiO_2-high ρ as a function of the distance from the silica particle surface normalized by the brush radius of gyration ($R_{g,b}$). The effective brush thickness h_{eff}, defined at $\varphi_t = 0.05$, represents the penetration depth of the tracer into the brush. (c) Effective particle size ($d_{eff} = d_0 + 2h_{eff}$) obtained from SCFT calculations as a function of tracer molecular weight for SiO_2 (triangles), SiO_2-low ρ:PS (circles), and SiO_2-high ρ:PS (squares). (d) Interparticle distance of grafted NPs normalized by that of SiO_2 NPs for dPS (49k, open symbols) and dPS (532k, closed symbols) as a function of the volume fraction of silica.

a result, the effective particle size in PS matrices containing NPs with high ρ increases to $d_{eff} = d_0 + 2h_{eff}$ relative to the hard NP case. Thus, the additional crowding imposed by the impenetrable brush layer should be taken into account when describing dynamics in PNCs.

As shown in Figure 5c, the effective particle size of SiO_2-low ρ is independent of the tracer molecular weight (i.e., $d_{eff} = d_0$) in the limit of low molecular weights; however, a weak dependence is observed at high molecular weight as noted by the increase in effective size for M_n^t = 532k. However, d_{eff} for SiO_2-high ρ in a PS matrix increases strongly with tracer molecular weight, resulting in a reduction of the interparticle spacing. The confinement size imposed by the impenetrable objects can be approximated by assuming a random distribution of NPs in 3D with an average interparticle spacing given by ID $= d_0\,[(2/(\pi\phi_{silica}))^{1/3}(\exp(\ln\sigma)^2) - 1]$, where d_0 is the number-average particle diameter and σ is the polydispersity of nanoparticles.[14] Using the SCFT results, the contribution due to the limited penetration into the brush can be taken into account to define an effective interparticle distance, ID_{eff} = ID $- 2h_{eff}$. To understand the dependence of the effective interparticle distance on the grafting density and the tracer molecular weight, the normalized interparticle distance ID_{eff} (grafted NP)/ ID_{eff} (hard NP), for dPS(49k) and dPS(532k) is plotted as a function of volume fraction of silica in Figure 5d. At low tracer molecular weight dPS(49k) the dependence of ID_{eff} on the grafting density is not observed (low grafting density) or its reduction is less than ~10% (high grafting density), whereas for high tracer molecular weight, dPS(532k), the effective ID decreases very strongly for NP systems with high ρ. When the brush structure impedes tracer penetration, the confinement between NPs increases which in turn impedes tracer diffusion as detailed below.

As grafting density increases, excluded volume from steric repulsion of crowded chains also increases, expelling polymer chains from the brush region and increasing the effective particle size ($d_{eff} > d_0$).[28] Although grafted NPs with low grafting density can exhibit good dispersion in a polymer matrix due to favorable wetting, polymer dynamics in PNCs containing grafted NPs is similar to the hard NP case ($d_{eff} \approx d_0$) as shown in the inset of Figure 6. By defining a new confinement parameter ($ID_{eff}/2R_g$) that incorporates wetting

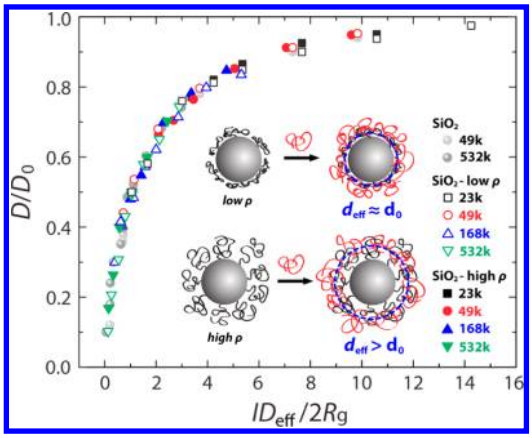

Figure 6. The reduced diffusion coefficient (D/D_0) of dPS (M_w = 23k, 49k, 168k, and 532k) as a function of the confinement parameter $ID_{eff}/2R_g$ yields a master curve; gray shaded circle (SiO_2:PS), open (SiO_2-low ρ:PS), and solid (SiO_2-high ρ:PS), symbols. The inset illustrates the NPs with low (top) and high (bottom) grafting density, showing the effective particle size depending on the grafting density.

and expulsion from the brush, the reduced diffusion coefficient (D/D_0) plotted against the confinement parameter collapses onto a master curve (Figure 6) for hard NPs and grafted NPs with low and high grafting density. This universal scaling behavior for D/D_0 over a wide range of $ID_{eff}/2R_g$, suggests a profound influence on polymer diffusion by affecting the characteristic length scale of NP separation relative to probe size. Namely, weak slowing down of polymer diffusion is observed under low confinement ($ID_{eff}/2R_g \approx 10$ or greater). As confinement increases, the reduced diffusion coefficient initially decreases gradually, and then much more strongly for $ID_{eff}/2R_g < 2$. Using an analytical model, Meth et al. recently showed that the diffusion of spheres through a cylinder captured the slowing down of polymer diffusion in nanocomposites at low loading, suggesting that the excluded volume effect plays a dominant role in the long-range slowing down at low confinement conditions.[29] However, at high loadings ($ID_{eff}/2R_g < 5$) this model underestimates the reduction of polymer diffusion possibly because chain conformation perturbations due to confinement are not taken into account. For example, tracer chains should lose conformational entropy

dx.doi.org/10.1021/ma500235v | Macromolecules 2014, 47, 2404−2410

upon squeezing between adjacent NPs for $ID_{eff} < \sim 2R_g$. While the current master curve is consistent with our previous one, these new studies define the importance of the brush structure as controlled by the surface grafting density and tracer molecular weight on the universal scaling behavior of polymer diffusion and provide guidelines for designing polymer nanocomposites with enhanced dispersion of NPs as well as tunable polymer dynamics (e.g., polymer processing). Moreover, the importance of confinement between NPs on polymer diffusion demonstrates the importance of entropic contributions. This view is consistent with a recent coarse-grained molecular dynamics simulation study that showed slowing down of unentangled polymers confined by nonattractive nanoparticles.[30]

SUMMARY

In summary, the architecture of polymer brushes grafted to NPs can be used to tune the diffusion of polymers in polymer nanocomposites. Namely, at low grafting density and low tracer molecular weight, polymers are able to penetrate the brush and diffusion is similar to the hard NP case. However, at high grafting density and high tracer molecular weight, the diffusing polymer is unable to penetrate the crowed brush because it will lose conformational entropy. In this case, the diffusing polymer is more strongly confined and the effective particle diameter is larger than the core size. Using this effective diameter, the interparticle distance is reduced and this stronger confinement leads to stronger slowing down, when compared to PNCs with hard NPs. Thus, without changing the loading of NPs, the confinement of polymers can be increased by tuning the brush architecture. By investigating high molecular weight tracer diffusion, the present study shows that both wet (penetrable brush) and dry (excluded brush) brush conditions are possible for grafted NPs and entangled chains. Tracer diffusion studies in nanocomposites provides new insight into how confinement affects polymer dynamics over long times (i.e., longer than reptation time), and will impact the interpretation of rheological properties that depend on the same fundamental properties (e.g., friction coefficient).

ASSOCIATED CONTENT

Supporting Information

Electron micrographs of a cross-section of PNCs and full self-consistent field theory calculations showing volume fraction depth profiles of brush, matrix, and tracer. This material is available free of charge via the Internet at http://pubs.acs.org.

AUTHOR INFORMATION

Corresponding Author

*(R.J.C.) E-mail: composto@seas.upenn.edu.

Notes

The authors declare no competing financial interest.

ACKNOWLEDGMENTS

This research was primarily supported by the National Science Foundation NSF/EPSRC Materials World Network DMR-1210379 (R.J.C., K.I.W.), as well as EP/5065373/1 (N.C.) and Dupont Central Research and Development (R.J.C.). Support was also provided by the NSF/MRSEC-DMR 11-20901 (K.I.W., R.J.C.), and Polymer Programs DMR09-07493 (R.J.C.). M.J.A.H. acknowledges support from a National Research Council (NRC) Postdoctoral Associateship at the NIST Center for Neutron Research. The identification of commercial products or experimental methods does not imply endorsement by the National Institute of Standards and Technology nor does it imply that these are the best for the purpose. Helpful discussions with Prof. K. Schweizer (UIUC) and Dr. J. Meth (DuPont) are acknowledged. Ion scattering studies were assisted by Dr. D. Yates.

REFERENCES

(1) Stoykovich, M. P.; Kang, H.; Daoulas, K. Ch.; Liu, G.; Liu, C. -C.; de Pablo, J. J.; Muller, M.; Nealey, P. F. *ACS Nano* **2007**, *1*, 168−175.
(2) Starzyk, A.; Cieplak, M. *J. Chem. Phys.* **2011**, *135*, 235103.
(3) Shin, K.; Obukhov, S.; Chen, J. T.; Huh, J.; Hwang, Y.; Mok, S.; Dobriyal, P.; Thiyagarajan, P.; Russell, T. P. *Nat. Mater.* **2007**, *6*, 961−965.
(4) Si, L.; Massa, M. V.; Dalnoki-Veress, K.; Brown, H. R.; Jones, R. A. L. *Phys. Rev. Lett.* **2005**, *94*, 127801.
(5) Choi, J.; Hore, M. J. A.; Meth, J. S.; Clarke, N.; Winey, K. I.; Composto, R. J. *ACS Macro Lett.* **2013**, *2*, 485−490.
(6) Jouault, N.; Moll, J. F.; Meng, D.; Windsor, K.; Ramcharan, S.; Kearney, C.; Kumar, S. K. *ACS Macro Lett.* **2013**, *2*, 371−374.
(7) Lin, C. C.; Gam, S.; Meth, J. S.; Clarke, N.; Winey, K. I.; Composto, R. J. *Macromolecules* **2013**, *46*, 4502−4509.
(8) Kumar, S. K.; Jouault, N.; Benicewicz, B.; Neely, T. *Macromolecules* **2013**, *46*, 3199−3214.
(9) Choi, J.; Hui, C. M.; Schmitt, M.; Pietrasik, J.; Margel, S.; Matyjaszewski, K.; Bockstaller, M. R. *Langmuir* **2013**, *29*, 6452−6459.
(10) Li, Y.; Tao, P.; Viswanath, A.; Benicewicz, B.; Schadler, L. S. *Langmuir* **2013**, *29*, 1211−1220.
(11) Harton, S. E.; Kumar, S. K.; Yang, H.; Koga, T.; Hicks, K.; Lee, H.; Mijovic, J.; Liu, M.; Vallery, R. S.; Gidley, D. W. *Macromolecules* **2010**, *43*, 3415−3421.
(12) Krutyeva, M.; Wischnewski, A.; Monkenbusch, M.; Willner, L.; Maiz, J.; Mijangos, C.; Arbe, A.; Colmenero, J.; Radulescu, A.; Holderer, O.; Ohl, M.; Richter, D. *Phys. Rev. Lett.* **2013**, *110*, 108303.
(13) Gam, S.; Meth, J. S.; Zane, S. G.; Chi, C.; Wood, B. A.; Seitz, M. E.; Winey, K. I.; Clarke, N.; Composto, R. J. *Macromolecules* **2011**, *44*, 3494−3501.
(14) Gam, S.; Meth, J. S.; Zane, S. G.; Chi, C.; Wood, B. A.; Winey, K. I.; Clarke, N.; Composto, R. J. *Soft Matter* **2012**, *8*, 6512−6520.
(15) Hore, M. J. A.; Composto, R. J. *Macromolecules* **2012**, *45*, 6078−6086.
(16) Chantawansri, T. L.; Hur, S.-M.; Garcia-Cervera, C. J.; Ceniceros, H. D.; Fredrickson, G. H. *J. Chem. Phys.* **2011**, *134*, 244905.
(17) Ceniceros, H. D.; Fredrickson, G. H. *Multiscale Model. Simul.* **2004**, *2*, 452−474.
(18) Choi, J.; Dong, H.; Matyjaszewski, K.; Bockstaller, M. R. *J. Am. Chem. Soc.* **2010**, *132*, 12537−12539.
(19) Choi, J.; Hui, C. M.; Pietrasik, J.; Dong, H.; Matyjaszewski, K.; Bockstaller, M. R. *Soft Matter* **2012**, *8*, 4072.
(20) Matyjaszewski, K.; Miller, P. J.; Shukla, N.; Immaraporn, B.; Gelman, A.; Luokala, B. B.; Siclovan, T. M.; Kickelbick, G.; Vallant, T.; Hoffmann, H.; Pakula, T. *Macromolecules* **1999**, *32*, 8716−8724.
(21) Composto, R. J.; Walters, R. M.; Genzer, J. *J. Mater. Sci. Eng. Res.* **2002**, *38*, 107−180.
(22) Chevigny, C.; Dalmas, F.; Cola, E. D.; Gigmes, D.; Bertin, D.; Boue, F.; Jestin, J. *Macromolecules* **2011**, *44*, 122−133.
(23) Crank, J. *The Mathematics of Diffusion*, 2nd ed.; Clarendon Press: Oxford, U.K., 1975.
(24) Green, P. F.; Mills, P. J.; Kramer, E. J. *Polymer* **1986**, *27*, 1063−1066.
(25) Green, P. F. *Soft Matter* **2011**, *7*, 7914−7926.
(26) Wijmans, C. M.; Zhulina, E. B. *Macromolecules* **1993**, *26*, 7214−7224.
(27) Choi, J.; Bockstaller, M. R. *Polymer Science: A Comprehensive polymer science*, 2nd ed.; Elsevier: Amsterdam, 2012; Vol. 7, pp 313−326.

(28) Wu, T.; Efimenko, K.; Viček, P.; Šubr, V.; Genzer, J. *Macromolecules* **2003**, *36*, 2448−2453.
(29) Meth, J. S.; Gam, S.; Choi, J.; Lin, C.-C.; Composto, R. J.; Winey, K. I. *J. Phys. Chem. B* **2013**, *117*, 15675−15683.
(30) Li, Y.; Kroger, M.; Liu, W. K. *Soft Matter* **2014**, *10*, 1723−1737.